MAPPING THE DARK MATTER THROUGH THE CMB DAMPING TAIL

WAYNE HU

Department of Astronomy and Astrophysics, University of Chicago, Chicago, IL 60637

Draft version February 1, 2008

ABSTRACT

The lensing of CMB photons by intervening large-scale structure leaves a characteristic imprint on its arcminute-scale anisotropy that can be used to map the dark matter distribution in projection on degree scales or $\sim 100 h^{-1}$ Mpc comoving. We introduce a new algorithm for mass reconstruction which optimally utilizes information from the weak lensing of CMB anisotropies in the damping tail. Individual degree-scale mass structures can be recovered with high signal-to-noise from a foreground-free CMB map of arcminute scale resolution, specifically with a FWHM beam $< 5'$ and a noise level < 15 (10^{-6}-arcmin) or 41 (μK-arcmin).

Subject headings: cosmic microwave background – dark matter — large scale structure of universe

1. INTRODUCTION

It is well-known from the study of the weak gravitational lensing of faint galaxies that the distortion of background images can be used to map the intervening mass distribution in projection (Tyson et al. 1990; Kaiser & Squires 1993). As the most distant background image available, maps of the CMB temperature distribution provide a unique opportunity to map the distribution of dark matter. They provide information about structures on the largest linear scales in the high redshift universe (Zaldarriaga & Seljak 1999) and hence complement information from weak lensing surveys. The main difficulty is that unlike an image of background galaxies, the temperature distribution of the CMB is to good approximation a Gaussian random field with no characteristic shape.

Algorithms in the literature for extracting the intervening mass distribution from lensed CMB maps have shown the potential for statistical detections by the Planck satellite.[1] Bernardeau (1998) considered the distortion to the Hessian of the temperature field. Zaldarriaga & Seljak (1999) considered distortions to the product of gradients of the temperature field. In neither case is it possible to extract high signal-to-noise maps of the dark matter.

Recently Zaldarriaga (2000) showed that the damping tail of CMB anisotropies (see e.g. Hu & White 1997) exhibits enhanced lensing effects in the four-point function. Indeed even the two-point function or power spectrum shows enhanced effects in this region due to the multitude of acoustic peaks and the sharp decline in intrinsic power associated with damping (Metcalf & Silk 1997).

Hu (2001) showed that there is a quadratic estimator that recovers all of the information in the four-point function about the mass distribution on large scales. Even for experiments like Planck that only partially resolve the damping tail, this estimator reduces the noise variance of the recovered projected mass power spectrum by over an order of magnitude. Planned experiments to measure arcminute-scale secondary CMB anisotropies can potentially use this statistic to map the dark matter at high signal-to-noise.

We begin in §2 by reviewing the effect of lensing on CMB temperature maps. In §3, we describe the reconstruc-

[1] http://astro.estec.esa.nl/SA-general/Projects/Planck

tion algorithm and test it with realizations of the CMB temperature field and instrumental noise. We discuss observational strategies for optimizing the reconstruction in §4. For illustration purposes we use a flat ΛCDM cosmology throughout with parameters $\Omega_c = 0.3$, $\Omega_b = 0.05$, $\Omega_\Lambda = 0.65$, $h = 0.65$, $n = 1$ and $\delta_H = 4.2 \times 10^{-5}$.

2. LENSING

Weak lensing of the CMB photons by the intervening mass distribution remaps the primary temperature field $\tilde\Theta(\hat{\mathbf{n}})$ as a function of the directional vector $\hat{\mathbf{n}}$ on the sky as (e.g. Seljak 1996; Goldberg & Spergel 1999)

$$\Theta(\hat{\mathbf{n}}) = \tilde\Theta(\hat{\mathbf{n}} + \nabla\phi) , \tag{1}$$

where $\nabla\phi$ is the deflection angle which is related to the gravitational potential $\Psi(\mathbf{x}, D)$ as

$$\phi(\hat{\mathbf{n}}) = -2 \int dD \, \frac{D_A(D_s - D)}{D_A(D) \, D_A(D_s)} \Psi(D\hat{\mathbf{n}}, D) , \tag{2}$$

where D is the comoving coordinate distance along the line of sight and D_A is the comoving angular diameter distance associated with D. D_s is the coordinate distance to the last scattering surface. In a flat universe $D_A = D$. The projected potential $\phi(\hat{\mathbf{n}})$ has a power spectrum $C_L^{\phi\phi}$ which is itself a projection of the gravitational potential power spectrum (see e.g. Hu 2000, Eqn. 28). For the scales of interest here, the gravitational potential power spectrum is in the linear regime and hence $\phi(\hat{\mathbf{n}})$ is a Gaussian random field. The power spectrum of the deflection angles is given by $L(L+1)C_L^{\phi\phi}$ (see Fig. 1 for ΛCDM). For reference, the convergence power spectrum, or projected mass, is given by $[L(L+1)]^2 C_L^{\phi\phi}/4$. The rms deflection angle

$$\theta_{\rm rms}^2 = \sum_{L=1}^{\infty} \frac{2L+1}{4\pi} L(L+1) C_L^{\phi\phi} \tag{3}$$

is 2.6′ for this model but its coherence scale corresponds to the peak of the log power spectrum at $L \sim 60$ or a few degrees. Counterintuitively then, the arcminute scale structure of the CMB temperature field yields information about the mass distribution on much larger linear scales.
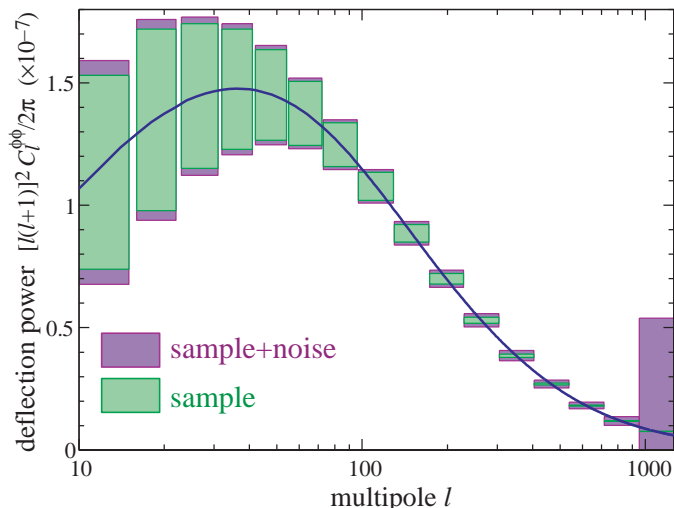
FIG. 1.— Lensing deflection power spectrum for the ΛCDM model. Error bars represent the total (sample plus noise) variance and sample variance from recovery from an area of $f_{\rm sky} = 0.1$ and an experiment with a beam of $\sigma = 1.5'$ and noise $w^{-1/2} = 10$ (10^{-6}-arcmin). Note that the errors for $L \lesssim 200$ are dominated by sample variance implying that the recovered map has high signal-to-noise.

The deflection power comes mainly from structures at redshifts $z \sim 1 - 2$ and scales of $k \sim$ few $\times 10^{-2}$ Mpc^{-1} (see Zaldarriaga & Seljak 1999, Fig. 7).

To simulate a lensed CMB map, one makes a Gaussian random realization of the unlensed CMB power spectrum $\tilde{C}_l$ and remaps the temperature field according to a random realization of the projected potential $C_L^{\phi\phi}$. Detector noise and residual foregrounds are then added as a realization of $C_l^{\rm noise}$. For detector noise and a finite beam of σ (FWHM) (Knox 1995)

$$C_l^{\rm noise} = w^{-1} e^{l(l+1)\sigma^2/8\ln 2}, \qquad (4)$$

with w^{-1} is the noise in units of $(\Delta T/T\text{-radian})^2$.

Because the deflection angles are small compared with the scale of the structures, the lensing effect is difficult to see directly in a map. To gain a better intuition for the nature of the effect, let us first consider lensing by a circularly symmetric Gaussian profile in projected mass with a scale of $5°$ and an amplitude corresponding to a $3°$ maximum deflection. As in the case of the weak lensing of faint galaxies, the distortion represents a tangential shearing of the image. Unlike the faint galaxy case, the source image is a Gaussian random field. Although the temperature map itself clearly shows evidence for lensing, the two point statistics of the CMB temperature field do not suffice to reconstruct the mass distribution of the lens.

3. RECONSTRUCTION

The case of the symmetric lens in Fig. 2 suggests that a statistic related to the Laplacian of the temperature field would trace the underlying mass distribution. The fact that both hot and cold spots are lensed alike washes out the signal in the Laplacian itself. Hu (2001) showed that a related statistic, the divergence of the temperature-weighted gradient of the map retains all of the information inherent in the four-point function (Zaldarriaga 2000). Here we consider its use in mapping the dark matter.
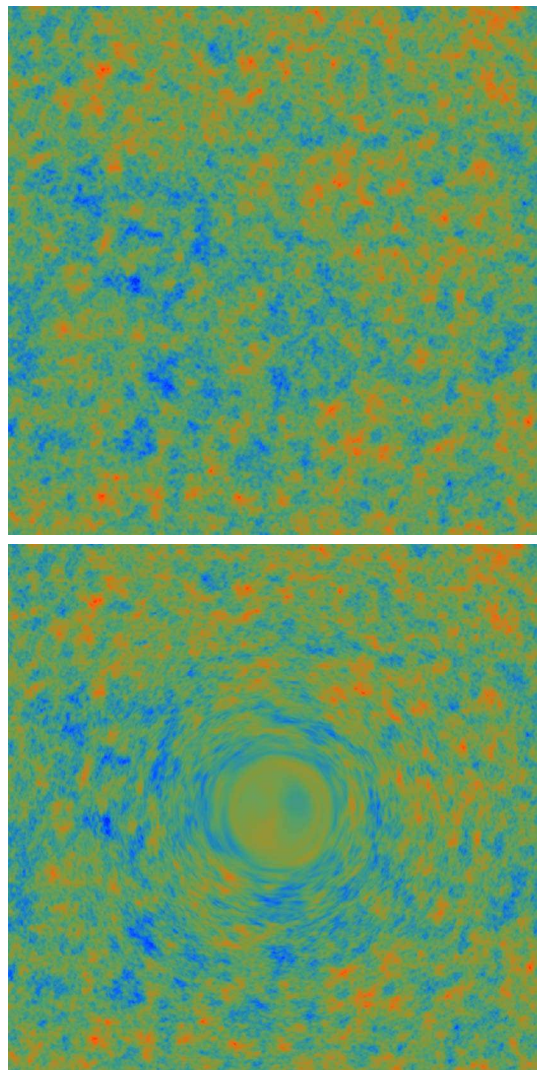

FIG. 2.— Top: A $32° \times 32°$ realization of the CMB temperature field. Bottom: A toy example of the lensing effect. A circularly symmetric projected mass with deflection angles comparable to the size of the structure. The distortion of the fine-scale anisotropy of the CMB traces the lensing structure on much larger scales.

We describe the technique for reconstructing the dark matter field on small sections of the sky $\theta_{\rm map} < 60°$ for which spherical harmonic analysis can be replaced by Fourier techniques. For the generalization to the curved sky see Hu (2001).

The first step is to take the gradient of the temperature map by filtering in the Fourier domain,

$$\mathbf{G}(\hat{\mathbf{n}}) = \int \frac{d^2l}{(2\pi)^2} i\mathbf{l} \frac{\tilde{C}_l}{C_l^{\rm tot}} \Theta(\mathbf{l}) e^{i\mathbf{l}\cdot\hat{\mathbf{n}}}, \qquad (5)$$

where $C_l^{\rm tot} = C_l + C_l^{\rm noise}$, C_l ($\tilde{C}_l$) is lensed (unlensed) power spectrum. Note that taking the gradient effectively high-pass filters the map. Next construct an explicitly high-pass filtered temperature map

$$W(\hat{\mathbf{n}}) = \int \frac{d^2l}{(2\pi)^2} \frac{1}{C_l^{\rm tot}} \Theta(\mathbf{l}) e^{i\mathbf{l}\cdot\hat{\mathbf{n}}}, \qquad (6)$$

to weight the gradient

$$\tilde{\mathbf{G}}(\hat{\mathbf{n}}) = W(\hat{\mathbf{n}})\mathbf{G}(\hat{\mathbf{n}}). \qquad (7)$$
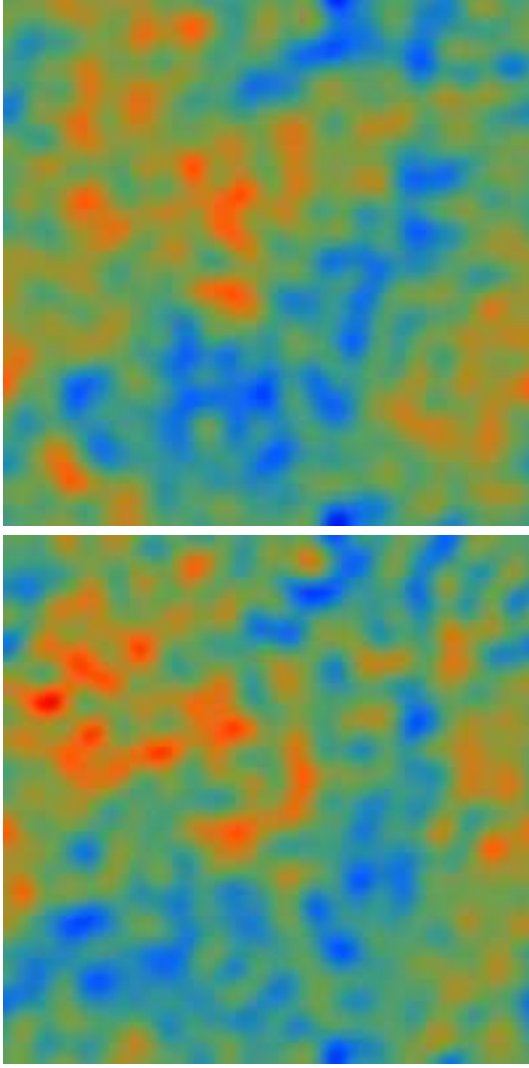
so that

$$\langle D(\mathbf{L})\rangle_{\mathrm{CMB}} = d(\mathbf{L}) = L\phi(\mathbf{L}),\qquad(12)$$

if

$$N_L^{-1} = \frac{1}{L^2}\int\frac{d^2 l_1}{(2\pi)^2}\frac{(\mathbf{L}\cdot\mathbf{l}_1\,\tilde{C}_{l_1} + \mathbf{L}\cdot\mathbf{l}_2\,\tilde{C}_{l_2})^2}{2C_{l_1}^{\mathrm{tot}}C_{l_2}^{\mathrm{tot}}}.\qquad(13)$$

Notice that the filters are designed so that the lensing effects in the Fourier domain add coherently such that the dot product above comes in as the square. This is a reflection of the optimization.

We show an example of this reconstruction on a $32° \times 32°$ field in Fig. (3) with detector noise added as appropriate for a beam of $\sigma = 1.5'$ and noise of $w^{-1/2} = 10$ $(10^{-6}$-arcmin) or $(27\mu\mathrm{K}$-arcmin) additionally low pass filtered to show $L \leq 150$ where the signal-to-noise is the highest. Alternately, Weiner filtering can be used to get a better visual impression of the fidelity of the map. In any case, the degree scale features in the map are recovered at good signal-to-noise.

In the idealization of an ensemble of CMB maps lensed by the *same* structure, $D(\mathbf{L})$ returns an unbiased estimate of the deflection map. However given that we only have one realization of the lensing per lens, it is important to understand the properties of the noise introduced by the Gaussian primary anisotropies themselves and the instrumental and/or foreground noise. Following Hu (2001),

$$\langle D^*(\mathbf{L})D(\mathbf{L}')\rangle = (2\pi)^2\delta(\mathbf{L}-\mathbf{L}')\left(L^2 C_L^{\phi\phi} + N_L\right),\quad(14)$$

so that N_L also plays the role of the noise power spectrum. A deflection power spectrum extracted from this statistic must remove this noise bias. As discussed in Hu (2001), the noise bias may alternately be eliminated by cross-correlating maps reconstructed from independent l-bands in the original lensed map.

Under the assumption of Gaussian statistics, the signal-to-noise per L in the deflection power spectrum is given by

$$\left(\frac{S}{N}\right)_L^2 = f_{\mathrm{sky}}\frac{2L+1}{2}\left(\frac{L^2 C_L^{\phi\phi}}{L^2 C_L^{\phi\phi} + N_L}\right)^2,\qquad(15)$$

and the precision with which the binned deflection power spectrum can be recovered by an experiment with a sky fraction of $f_{\mathrm{sky}} = 0.1$ $(\sim 4000\mathrm{deg}^2)$ and $\sigma = 1.5'$, $w^{1/2} = 10$ $(10^{-6}$-arcmin) is shown in Fig. 1. Also shown are the errors provided by sample variance alone. Since sampling errors dominate at $L \lesssim 150$, the recovered map has good signal-to-noise on those characteristic structures. This is independent of the actual sky fraction covered by the experiment.

4. DISCUSSION

The statistic introduced here utilizes CMB structures in the *arcminute* regime of the damping tail to map the dark matter on *degree* scales. As with the weak lensing of faint galaxies, image distortions manifest on small angular scales are used to reconstruct the mass on a much larger scale. Mapping the dark matter distribution therefore requires high resolution, high signal-to-noise maps of the
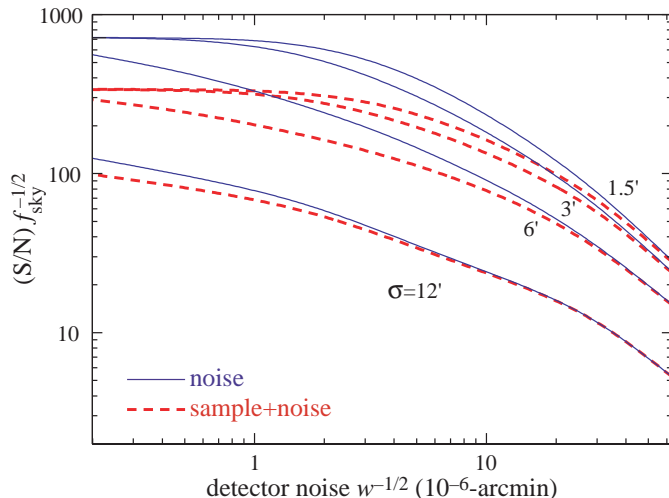

FIG. 3.— Top: A $32° \times 32°$ realization of the deflection field in the ΛCDM model. Bottom: Recovery of the deflection field with a $\sigma = 1.5'$ beam (FWHM) and detector noise of $w^{-1/2} = 10$ $(10^{-6}$-arcmin).

Finally take a filtered divergence of this field in the Fourier domain

$$D(\hat{\mathbf{n}}) = -\int\frac{d^2 L}{(2\pi)^2}\frac{N_L}{L}i\mathbf{L}\cdot\tilde{\mathbf{G}}(\mathbf{L})e^{i\mathbf{L}\cdot\hat{\mathbf{n}}}.\qquad(8)$$

The normalization factor N_L/L may be chosen so that $D(\hat{\mathbf{n}})$ averaged over an ensemble of CMB realizations recovers the deflection field

$$d(\hat{\mathbf{n}}) \equiv \int\frac{d^2 L}{(2\pi)^2}L\phi(\mathbf{L})e^{i\mathbf{L}\cdot\hat{\mathbf{n}}}.\qquad(9)$$

To determine N_L consider the operations directly in the Fourier domain,

$$D(\mathbf{L}) = \frac{N_L}{L}\int\frac{d^2 l_1}{(2\pi)^2}(\mathbf{L}\cdot\mathbf{l}_1\,\tilde{C}_{l_1} + \mathbf{L}\cdot\mathbf{l}_2\,\tilde{C}_{l_2})\frac{\Theta_{l_1}\Theta_{l_2}}{2C_{l_1}^{\mathrm{tot}}C_{l_2}^{\mathrm{tot}}},\quad(10)$$

where $\mathbf{l}_2 = \mathbf{L} - \mathbf{l}_1$. Taylor expanding Eqn. (1) for the lensing one obtains (Hu 2000)

$$\Theta(\mathbf{l}) = \tilde{\Theta}(\mathbf{l}) - \int\frac{d^2 l_1}{(2\pi)^2}\Theta(\mathbf{l}_1)\phi(\mathbf{l}-\mathbf{l}_1)(\mathbf{l}-\mathbf{l}_1)\cdot\mathbf{l}_1,\quad(11)$$

FIG. 4.— Signal-to-noise as a function of detector noise, beam and sky fraction $f_{\rm sky}$. Solid lines include both sample and Gaussian noise (primary CMB and instrumental) variance; dashed lines include only Gaussian noise variance. The signal-to-noise drops off rapidly for $w^{-1/2} > 15$ (10^{-6}-arcmin) and FWHM beams $\sigma > 5'$.

CMB anisotropies themselves. Conversely, though a wide field of at least several degrees on the side is required to map the full extent of the structures expected, the statistic essentially high pass filters the input CMB maps. A true map that retains correlations across these scales is not necessary.

To see how an observing strategy might be optimized for mapping the dark matter, let us consider the trade-offs between sky coverage, instrumental noise and beam. Because this statistic is a quadratic function of the temperature fluctuation data, the balance differs from the usual case. In Fig. 4, we show the total signal-to-noise in the measurement of the deflection power spectrum (summed in quadrature over L) of an experiment as a function of these parameters. We consider separately the case of noise variance from the Gaussian random primary anisotropies and detector noise alone and combined with the sample variance of the lensing fields. When the former exceeds the latter, a high signal-to-noise map of the structures results. Because this is an integrated statistic, the characteristic signal-to-noise for large-scale features is much higher (see Fig. 1).

Compare the steep increase in the signal-to-noise as the detector noise is reduced with the shallow increase with sky coverage of $f_{\rm sky}^{1/2}$. Up until $w^{-1/2} \sim 10$ (10^{-6}-arcmin), observing time is best spent going deep rather than wide. Beyond this point, the intrinsic noise variance provided by the primary CMB anisotropies themselves begins to dominate and saturate the signal-to-noise. If the goal is to produce a high signal-to-noise map of structures, then going down to $w^{-1/2} \sim 1$ (10^{-6}-arcmin) can achieve substantially improved maps of the finer scale structures in the map. Another crucial factor is the beam size. To resolve the structures that best trace the lensing, a beam of $\sigma < 5'$ is required and it is not until $\sigma \sim 1' - 2'$ that the gains saturate. If foregrounds are not removed from the map through their spatial coherence and/or frequency dependence then this balance can shift to larger angular scales and more sky coverage. For the 1.5', 10 (10^{-6}-arcmin)

baseline experiment, inclusion of Gaussian random noise from the Sunyaev-Zel'dovich and Vishniac effects in $C_l^{\rm tot}$ imply a relative degradation in signal-to-noise of $\sim 10\%$ and $\sim 1\%$ (for $\tau = 0.1$) respectively and so do not require substantial reoptimization.

A high signal-to-noise map of the dark matter in projection can also be used to pull out tracers of the large-scale structure of the universe in other maps through cross-correlation. Examples include secondary anisotropies such as the integrated Sachs-Wolfe and Sunyaev-Zel'dovich effects (Goldberg & Spergel 1999; Seljak & Zaldarriaga 1998; Cooray & Hu 2000). One can show that the statistic employed here retains all of the information in the full bispectrum of the secondary-lensing-primary correlation and so is the optimal statistic to measure these correlations.

The filters used to reconstruct the dark matter map formally require as input the power spectrum of the CMB *before* lensing. The lensed CMB power spectrum will of course be measured to exquisite precision by CMB satellites and by the input temperature map themselves. Employing the lensed CMB power spectrum in the filter or an otherwise slightly incorrect assumption simply degrades the signal-to-noise by a correspondingly small amount but does not introduce spurious structures in the ensemble-averaged recovery. They appear as a calibration error for the mass map. Indeed in the context of a parameterized cosmology the unlensed CMB power spectrum may itself be reconstructed from the observed spectrum. For a non-uniform survey geometry, with perhaps foreground-contaminated regions removed, more sophisticated techniques than the Fourier-transform filtering scheme employed here will have to be developed. These complications should not present an insurmountable obstacle to the goal of mapping the dark matter in projection at intermediate redshifts.

REFERENCES

Bernardeau, F. 1998, A&A, 338, 375.
Cooray, A.R. Hu, W. 2000, ApJ, 534, 533.
Goldberg, D.M. Spergel, D.N. 1999, Phys. Rev. D, 59, 103002.
Hu, W. 2000, Phys. Rev. D, 62, 043007.
Hu, W. 2001, Phys. Rev. D, in press, astro-ph/0105117.
Hu, W. White, M. 1997, ApJ, 479, 568.
Kaiser, N. Squires, G. 1993, ApJ, 404, 441.
Knox, L. astro-ph/9504054, Phys. Rev. D, 52, 4307.
Metcalf, R.B. Silk, J. 1997, ApJ, 489, 1.
Seljak, U. 1996, ApJ, 463, 1.
Seljak, U. Zaldarriaga, M. 1999, Phys. Rev. D, 60, 043504.
Tyson, J.A. Wenk, R.A. Valdes, F. 1990, ApJ, 349, 1.
Zaldarriaga, M. 2000, Phys. Rev. D, 62, 063510.
Zaldarriaga, M. Seljak, U. 1999, Phys. Rev. D, 59, 123507.